HHS Public Access

Author manuscript

Toxicol Appl Pharmacol. Author manuscript; available in PMC 2018 May 31.

Published in final edited form as:

Toxicol Appl Pharmacol. 2016 October 01; 308: 46–58. doi:10.1016/j.taap.2016.07.015.

Activating transcription factor 4 underlies the pathogenesis of arsenic trioxide-mediated impairment of macrophage innate immune functions

Ritesh K. Srivastava[a], **Changzhao Li**[a], **Yong Wang**[b], **Zhiping Weng**[a], **Craig A. Elmets**[a], **Kevin S. Harrod**[c], **Jessy S. Deshane**[b,**], and **Mohammad Athar**[a,*]

[a]Department of Dermatology and Skin Diseases Research Center, University of Alabama at Birmingham, Birmingham, AL, USA

[b]Department of Medicine, University of Alabama at Birmingham, Birmingham, AL, USA

[c]Department of Anesthesiology and Perioperative Medicine, University of Alabama at Birmingham, Birmingham, AL, USA

Abstract

Chronic arsenic exposure to humans is considered immunosuppressive with augmented susceptibility to several infectious diseases. The exact molecular mechanisms, however, remain unknown. Earlier, we showed the involvement of unfolded protein response (UPR) signaling in arsenic-mediated impairment of macrophage functions. Here, we show that activating transcription factor 4 (ATF4), a UPR transcription factor, regulates arsenic trioxide (ATO)-mediated dysregulation of macrophage functions. In ATO-treated $ATF4^{+/+}$ wild-type mice, a significant down-regulation of CD11b expression was associated with the reduced phagocytic functions of peritoneal and lung macrophages. This severe immunotoxicity phenotype was not observed in ATO-treated $ATF4^{+/-}$heterozygous mice. To confirm these observations, we demonstrated in Raw 264.7 cells that ATF4 knock-down rescues ATO-mediated impairment of macrophage functions including cytokine production, bacterial engulfment and clearance of engulfed bacteria. Sustained activation of ATF4 by ATO in macrophages induces apoptosis, while diminution of ATF4 expression protects against ATO-induced apoptotic cell death. Raw 264.7 cells treated with ATO also manifest dysregulated Ca^{++} homeostasis. ATO induces Ca^{++}-dependent calpain-1 and caspase-12 expression which together regulated macrophage apoptosis. Additionally, apoptosis was also induced by mitochondria-regulated pathway. Restoring ATO-impaired Ca^{++} homeostasis in ER/mitochondria by treatments with the inhibitors of inositol 1,4,5-trisphosphate receptor (IP3R) and voltage-dependent anion channel (VDAC) attenuate innate immune functions of macrophages. These studies identify a novel role for ATF4 in underlying pathogenesis of macrophage dysregulation and immuno-toxicity of arsenic.

*Correspondence to: M. Athar, Department of Dermatology, University of Alabama at Birmingham, Birmingham, AL 35294-0019, USA. **Correspondence to: J. Deshane, Department of Medicine, University of Alabama at Birmingham, Birmingham, AL 35294-0019, USA.

Conflict of interest

The authors declare no conflict of interest.

Transparency document

The Transparency document associated with this article can be found, in online version.

Keywords

Apoptosis; Arsenic; ATF4; Macrophage functions; Ca^{++} homeostasis; UPR

1. Introduction

Arsenic exposure through contaminated drinking water is a worldwide public health problem (Brown et al., 2002; Abhyankar et al., 2012; McClintock et al., 2012). Its exposure has been associated with increased risk of cancer in kidney, skin, bladder, lung, prostate and other organs (Mink et al., 2008; Gibb et al., 2011; McClintock et al., 2012). In addition to its carcinogenic effects, arsenic also suppresses the immune system. As a consequence, elevated levels of arsenic in the environment can hinder innate immune responses against bacterial and viral infections. Illustrating this idea, a significant decrease in pulmonary antibacterial defense was noted in mice exposed to arsenic trioxide (ATO) (Aranyi et al., 1985; Burchiel et al., 2009). An exacerbated risk of influenza A (H1N1) infection and -associated lung function following arsenic exposure were also reported in other independent studies (Kozul et al., 2009a; Kozul et al., 2009b). ATO exposure enhanced human immunodeficiency virus type-1 (HIV-1) infection in an *in vitro* study (Nayak et al., 2007; Pion et al., 2007). Similarly, in a zebrafish model, 2–10 ppb arsenic levels in water augmented the viral load by 50-fold and bacterial load by 17-fold suggesting the immunosuppressive effects of arsenic (Nayak et al., 2007). Lower respiratory tract infections and diarrhea are more common in arsenic-exposed human populations, particularly among children from Bangladesh and other countries where high levels of arsenic in drinking water have been reported (Mazumder et al., 2000; Raqib et al., 2009; Rahman et al., 2011; Smith et al., 2011). Increased mortality from pulmonary tuberculosios has been reported in Chile from drinking arsenic-contaminated water (Smith et al., 2011).

The higher incidence of opportunistic infections, allergy and asthma in arsenic-exposed human populations likely results from failure to maintain an equilibrated immune response. In this regard, arsenic exposure has been shown to inhibit proliferative response of T cells and alters their cytokine secretion profiles (Biswas et al., 2008). Arsenic also reduces the proportion of T helper cell (CD4) relative to T cytotoxic cells (CD8) ratio (CD4/CD8) in exposed children (Soto-Pena et al., 2006). Pre-natal exposure to arsenic significantly reduces thymic function via oxidative stress and apoptosis (Ahmed et al., 2012) and alters DNA methylation (Kile et al., 2014), which collectively are thought to contribute to immunosuppression in childhood. Furthermore, impaired T cell functions have also been reported in experimental animals subjected to arsenic (Burchiel et al., 2009; Martin-Chouly et al., 2011). Cutaneous contact hypersensitivity response is impaired in mice exposed to arsenic (Patterson et al., 2004; Zhou et al., 2006), and chronic arsenic exposure of mice significantly decreases adhesion property and phagocytic activity of splenic macrophages (Bishayi and Sengupta, 2003).

In addition to the deleterious effects of environmental arsenic, ATO is a food and drug administration (FDA) approved chemotherapeutic agent and is used for the treatment of promyelocytic leukemia (PML) (Lengfelder et al., 2012). ATO treatment of patients with

multiple myeloma and colon cancer, as well as those with PML, has been reported to contribute to recurrent herpes simplex and herpes zoster virus infection (Tanvetyanon and Nand, 2004; Nouri et al., 2006; Yamakura et al., 2014; Cardenas et al., 2015). T cell mediated immunity is attenuated in these arsenic-treated cancer patients by induction of regulatory T cells (Tohyama et al., 2013).

The precise molecular mechanism by which arsenic impairs immune functions is yet to be defined. We demonstrated earlier that *in vitro* treatment of murine macrophage, Raw 264.7 cells with ATO diminished phagocytic functions. These effects were suggested to involve the unfolded protein response (UPR) signaling as 4-phenylbutyric acid (PBA), a chemical chaperone alleviated markers of UPR signaling, including GRP78, p-eIF2α, and CHOP, and afforded protection against ATO-mediated changes in these innate immune cells (Srivastava et al., 2013). ATF4 increases the expression of CHOP which is also a UPR transcriptional regulator that has been shown to play an important role in the pathogenesis and survival of mycobacterium in mouse macrophage cells (Lim et al., 2011). ATF4 plays key roles in diverse biological and patho-biological processes such as bone formation (Wang et al., 2012), hepatic steatosis (Jo et al., 2012) and glutamine-regulated cancer cell survival/apoptosis (Qing et al., 2012). Recent evidence indicates that ATF4 also participates in signaling of the toll like receptors 4 (TLR4), which in turn regulates cytokine production (Woo et al., 2009). In this study we determined that ATF4 is a central target involved in dampening of immune responses in arsenic exposed experimental animals. Our data provide novel *in vitro* and *in vivo* evidence for the involvement of ATF4 in ATO-mediated impairment of immune regulation.

2. Materials and methods

2.1. Cell culture

Mouse macrophage cell line Raw 264.7 (Cat no. TIB-71TM) were procured from American Type Culture Collection (Manassas, VA). Cells were cultured in DMEM medium containing 10% fetal bovine serum (FBS) (Sigma, St. Louis, MO) and 1% penicillin-streptomycin solution (Mediatech, Manassas, VA) at 37 °C in CO_2 incubator.

2.2. Animal studies

$ATF4^{+/+}$ wild-type (WT) and $ATF4^{+/-}$ heterozygous mice in the C57BL/6j background were purchased from Jackson laboratory (Bar Harbor, ME; http//www.jax.org). Selection of $ATF4^{+/-}$ heterozygous mice was based on the fact that $ATF4^{-/-}$ null mice are reported to be mostly neonatal lethal, and surviving animals are dwarf and display severe phenotypes in adulthood (Masuoka and Townes, 2002; Wang et al., 2009; Cornejo et al., 2013). To define the role of ATF4 on the susceptibility of animals for infection, twenty mice of each genotype (aged 5–6 weeks) were divided into two groups (10 mice/group). Group-1 received saline whereas group-2 received parental administration of ATO (50 μg/mouse in 200 μl PBS, intra-peritoneal; daily for 10 days). Each of these two groups was sub-divided into two subgroups. One subgroup received intratracheally (i.t.) saline, while the other subgroup received i.t. fluorescent *E. coli* bioparticles (2×10^7 *E. coli* in 30 μl PBS) as shown in Supplemental Fig. S1A. Fluorescent *E. coli* were administrated 3 h prior to euthanasia.

Briefly, the tongue of mice was gently extended in isoflurane-anesthetized mice, and the fluorescent *E. coli* was deposited into the oropharynx as described earlier (Bae et al., 2011). All animal experiments were performed according to the protocols approved by the Institutional Animal Care and Use Committee (IACUC) at the University of Alabama at Birmingham.

2.3. siRNA transfection

Raw 264.7 cells were transfected with either ATF4 siRNA (Sigma, St. Louis, MO) or scrambled siRNA obtained from Ambion, Life Technologies, (Grand Island, NY) at final concentration 10 nM. Transfection with siRNA was carried out using Opti-MEM-I reduced-serum medium (Invitrogen, Grand Island, NY) and lipofectamine 2000 transfection reagent (Sigma, St. Louis, MO).

2.4. Inflammatory cytokine levels

Inflammatory cytokine mRNA expression was determined by real time PCR using SYBR green methodology as described earlier (Srivastava et al., 2013). Primers used in this study are listed in Supplementary Table-SI.

2.5. Latex beads phagocytosis assay

Latex beads coated with fluorescently labeled rabbit-IgG was used as a probe to assess the phagocytic capacity of murine macrophages. The experiment was performed using Cayman's phagocytosis assay kit (IgG FITC) (Ann Arbor, MI) according to manufacturer's instructions. Briefly, Raw 264.7 cells transfected with either ATF4 or scrambled siRNA were treated with either saline or ATO (2 μM for 14 h). Cells were then incubated with 30 μl of latex beads coated with fluorescently labeled rabbit-IgG for 45 min. at 37 °C and then washed three times with assay buffer followed by incubation with trypan blue quenching solution. The engulfed fluorescent beads were quantitated through ELISA-based microplate reader at excitation 485 and emission at 535 nm. Cells incubated with latex beads at 4 °C instead of 37 °C served as negative controls (Srivastava et al., 2013).

2.6. Bacterial clearance assay

For studying the kinetics of clearance of engulfed bacteria by Raw 264.7 cells, we used fluorescently labeled opsonized *E. coli* (K-12 strain) bioparticles (Invitrogen, Grand Island, NY). ATF4 siRNA transfected Raw 264.7 cells were treated with either saline or ATO (2 μM for 14 h). Following these treatments, cells were incubated with at 37 °C for 2 h with *E. coli* bioparticles (Bioparticles:cell 50:1 ratio). The fluorescence of bioparticles conjugates that are bound to the surface but not internalized were quenched by trypan blue and imaged by fluorescent microscopy to capture the base line fluorescence of engulfed *E. coli* by Raw 264.7 cells at 2 h. After this, these cells were further incubated at 37 °C in CO_2 incubator to study the clearance of these engulfed *E. coli*. Cells were imaged again at 24 h to capture the differences in fluorescence of engulfed *E. coli* between various treatments of Raw 264.7 cells.

2.7. ATO treatment studies using peritoneal macrophages isolated from WT and ATF4$^{+/-}$ heterozygous mice

Peritoneal macrophages were harvested from the peritoneal cavity of WT and ATF4$^{+/-}$heterozygous mice by injecting 5 ml of sterile saline using 20-G needle. Cells were aspirated from the peritoneum and dispersed into 50 ml centrifuge tube. Following centrifugation at 400 ×*g* for 10 min, cells were resuspended in DMEM-F12 medium supplemented with 10% FBS, 1% penicillin and streptomycin. These peritoneal cells were then incubated in tissue culture plates at 37 °C and 5% CO_2 in incubator for 6–8 h to allow adherence of the cells. All non-adherent cells were removed by washing with PBS. The adherent cells were confirmed to be macrophages by morphology identification and immunostaining for F4/80, a known and widely-used marker of murine macrophage populations (Austyn and Gordon, 1981). These macrophages were then treated with either saline or ATO (2 μM for 14 h), processed for flow cytometry analysis of CD11b expression. Similar experiments were also performed by infecting these macrophages with fluorescently labeled *E. coli* bioparticles. For this study, following treatment with ATO, peritoneal macrophages from the two mouse genotypes were incubated with *E. coli* (Bacterial:cell, 50:1 ratio) at 37 °C for 2 h followed by incubation with trypan blue quenching solution. After this, these cells were further incubated at 37 °C for 24 h to study the clearance of these engulfed *E. coli*. Peritoneal macrophages were processed for flow cytometry analysis.

2.8. Isolation of lung tissue and flow cytometry analysis

Immune cells from the mouse lung tissues were isolated as described previously (Deshane et al., 2011). Briefly, contamination of isolated lung cells with blood was reduced by perfusion of the pulmonary circulation with PBS via the right ventricle following euthanasia and thoracotomy. Infiltrating leukocytes were isolated from minced lung tissue by treatment with collagenase-B (2 mg/ml, Roche, Indianapolis, IN) and DNase I (0.02 mg/ml, Sigma, St. Louis, MO) in Iscove's modified Dulbecco's medium (IMDM) supplemented with 1 mM sodium pyruvate, 2 mM L-glutamine, 10 μg/ml penicillin-streptomycin, 25 μM 2-mercaptoethanol and 0.1 mM non-essential amino acids (Life Technologies, Grand Island, NY) at 37 °C for 30 min. This was followed by the addition of an equal volume of IMDM containing 20% FBS. Cell suspensions were filtered using 40-μm cell strainer, washed with PBS, treated with ACK lysis buffer (Quality Biologicals Inc., Gaithersburg, MD) and then pretreated, for 20 min., in FACS staining buffer (PBS + 3% FBS) containing 2.0 μg/ml of the mAb 2.4G2 (BD Pharmingen, Franklin Lakes, NJ) at 4 °C. These cells were then stained to identify *E. coli* containing CD11b^{+} lung cells. Cells were washed twice with PBS before analysis. Flow cytometry acquisitions and analyses were carried out using Becton Dickinson LSR II with FACS Diva software (BD Biosciences, San Jose, CA). Data were further analyzed using FlowJo 10 (Tree Star, Ashland, OR) and percentages of CD11b^{+} lung cells which contained *E. coli* population were determined.

2.9. Detection of Ca^{++} levels

Fluo-4 Direct™ calcium assay kit (Invitrogen, Grand Island, NY) was used to determine the intracellular Ca^{++} levels as per instructions provided by the manufacturer. Briefly, 10,000 cells were plated in 96 well black bottom tissue culture plates for 24 h. Following ATO

treatments cells were washed with PBS and labeled with the Fluo-4 for 1 h (by incubating 30 min. at room temperature and 30 min. at 37 °C) in direct calcium assay buffer containing pro-benecid, which blocks the efflux of intracellular dyes. The fluorescence emitted by the cells at excitation wavelength 494 nm and emission wavelength 516 nm was recorded using ELISA-based microplate reader and expressed as mean of relative fluorescence intensity.

2.10. Protein quantification and western blot analysis

Protein quantification and western blot analysis were performed as described earlier (Srivastava et al., 2013). Cell lysates from ATO-treated cells were prepared using an ice cold lysis buffer, followed by centrifugation at 5000 rpm for 10 min to obtain a clear supernatant. Protein concentrations were determined using a DC kit (Bio-Rad, Hercules, CA). Equal amounts of protein lysates were mixed with 4× sample buffer boiled for 5 min at 95 °C and subjected to SDS-PAGE. The separated proteins were electrophoretically transferred to polyvinylidene difluoride membrane and then nonspecific sites were blocked with 5% nonfat dry milk in Tris buffer saline tween-20 (TBST) for 1 h at room temperature, followed by probing with primary antibody overnight at 4 °C. After washing, the membranes were incubated for 1.5 h–2 h with HRP conjugated secondary antibody (Pierce, Thermo Fisher Scientific, Pittsburg, PA). The blots were developed with enhanced chemiluminescence (ECL) according to manufacturer's instructions (Amersham Bioscience, Piscataway, NJ). Primary antibodies employed in this study are listed in Supplementary Table-SII.

2.11. Mitochondrial ROS (mROS)

mROS generation was assessed using MitoSOX red mitochondrial superoxide indicator dye (Invitrogen, Grand Island, NY) following manufacturer's protocol. Images of mROS production were captured using upright fluorescence microscopy (Olympus1X-S8F2, Japan).

2.12. ATP determination

ATP concentrations were determined using an ATP determination kit (Invitrogen, Grand Island, NY). Briefly, 2.5×10^6 cells were plated to 100 mM disc and allow them to adhere for 24 h. Cells were then treated with different concentrations of ATO (0.5–2 μM) for 24 h, followed by cell lysis. Assays were performed according to manufacturer's protocol.

2.13. Mitochondrial membrane potential (MMP)

MMP was detected using a cationic dye JC-1 (Sigma, St. Louis, MO). In intact mitochondria, JC-1 forms aggregates emitting red fluorescence, whereas loss of MMP leads to accumulation of JC-1 monomer that emit green fluorescence. Following various treatments, cells were incubated with JC-1 dye (10 μM) for 15 min at 37 °C followed by PBS wash. Cells were imaged and analyzed using upright fluorescence microscopy to assess the changes in the ratio of red (dye aggregates) to green (monomer) fluorescence.

2.14. Immunofluorescence (IF) staining

Immunofluorescence staining was performed as described earlier (Srivastava et al., 2014). Following ATO treatments, cells were washed with PBS, fixed in paraformaldehyde (4%)

for 10 min, permeabilized with Triton X-100 (0.5%) for 10 min followed by PBS wash, and blocked (1 h) with bovine serum albumin (2%). Cells were then incubated with primary antibodies overnight at 4 °C. After washing with PBS (three times), cells were incubated with fluorescein-conjugated secondary antibodies for 1.5 h at room temperature and then rinsed with PBS. These cells were incubated with DAPI at room temperature to counterstain cell nuclei and examined with upright fluorescence microscopy (Olympus1X-S8F2, Japan) or confocal microscopy (Zeiss LSM 710 confocal software 63× water corrected objective). In some experiments mitotracker dye was used to stain mitochondria performed before fixing.

2.15. Flow cytometry analysis of cell death

Cell death was measured by assessing subG0 populations of cell cycle as described earlier (Srivastava et al., 2014). Briefly, Raw 264.7 cells were seeded in 6-well plates and incubated overnight. Following various treatments cells were detached from plates with trypsin/EDTA, washed in PBS, and fixed with methanol for 4 h. Cells were again washed with PBS and incubated with RnaseA (Sigma, St. Louis, MO) at 37 °C for 1 h. Cells were pelleted by centrifugation and suspended in DNA staining solution, propidium iodide (10 μg/ml) (Sigma, St. Louis, MO) for 1 h and processed for flow cytometry analysis. Data were evaluated as percentage of cells present in different phases of the cell cycle.

2.16. Terminal deoxynucleotidyl transferase dUTP nick end labeling assay

TUNEL assays were performed by using the in situ DNA fragmentation assay Kit (Roche Diagnostics, Indianapolis, IN) according to the manufacturer's instructions. Briefly, cells were treated with ATO for 24 h, followed by a PBS wash, methanol fixing, and permeabilization with 0.1% Triton X-100. Cells were then washed three times and layered with 50 μM TUNEL reaction mixture, incubated for 1 h at 37 °C in a humid chamber, and visualized using fluorescence microscopy.

2.17. Cell fractionation

Cytoplasmic and mitochondrial extracts from ATO-treated and saline-treated cells were prepared as described earlier (Attardi and Ching, 1979). Briefly, harvested cells were suspended in ice-cold cell homogenization medium (150 mM $MgCl_2$, 10 mM KCL, 10 mM Tris HCl, pH −6.7). After homogenization, nuclei were collected by centrifugation for 5 min at 1000 ×g. The supernatant was subsequently subjected to centrifugation at 5000 ×*g* to collect the mitochondrial pellet. The mitochondrial pellet was suspended in mitochondrial suspension medium (0.25 M sucrose, 10 mM Tris-base, pH −7) for further processing and were analyzed by western blot analysis.

2.18. Statistical analysis

Data are expressed as mean ± standard error of mean (SEM). Data were analyzed for statistical significance using unpaired Student's *t*-test for comparison between two groups or one-way analysis of variance (ANOVA) followed by either Dunnett's or Bonferroni post-hoc test to compare multiple groups. Two-way ANOVA with Bonferroni post-test comparison was performed between genotypes (WT and $ATF4^{+/-}$ heterozygous mice) and treatment

groups. The statistical analysis was performed using GraphPad Prism, version 6.00. In all case, $P < 0.05$ was considered as significant.

3. Results

3.1. ATO-mediated inhibition of cytokines production, bacterial engulfment and clearance in murine macrophages are ATF4-dependent

ATF4 is one of the key transcription factors regulating UPR signaling (Cao and Kaufman, 2012). Following ER stress, there is preferential translation of ATF4, which then translocates to the nucleus where ATF4 directs transcription of UPR regulatory genes (Walter and Ron, 2011). In this study, we first confirmed that ATO treatment induces nuclear translocation of ATF4 and its downstream target CHOP in peritoneal macrophages isolated from WT mice, and in Raw 264.7 cells (Fig. 1A and Supplemental Fig. S1B).

Next we assessed cytokine gene expression in ATO-treated Raw 264.7 cells upon treatment with ATO. There was a significant ($P < 0.05$) reduction in mRNA expression of IL-1β, TNFα, IL-10 and TGF-β upon ATO treatment compared to saline-treated control cells (Fig. 1B). However, these cytokines were significantly induced in lipo-polysaccharides (LPS)-stimulated Raw 264.7 cells. LPS was used as a positive control in this experiment. ATO-treated Raw 264.7 cells also manifested significantly ($P < 0.05$) reduced engulfment of fluorescently labeled latex beads (Fig. 1C) and were not efficient in clearing the engulfed bacterial particles load (Fig. 1D). The presence of fluorescent tagged opsonized bacterial particles could be visualized over a period of 24 h in ATO-treated cells, whereas saline-treated control Raw 264.7 cells cleared almost all the fluorescence tagged *E. coli* bioparticles within this time (Fig. 1D and Supplementary Fig. S2A & S2B). These results were confirmed further by flow cytometry analysis (Supplementary Fig. S2C).

To investigate the role of ATF4 in ATO-mediated impairment of macrophage functions, we knocked down ATF4 expression in Raw 264.7 cells by siRNA transfection. siRNA transfection resulted in 70% reduction of ATF4 mRNA and similar reduction of ATF4 protein compared to scrambled (negative control) siRNA-transfected cells (Supplementary Fig. S3A). ATF4 knockdown was further confirmed by downregulation of its downstream target proteins CHOP and GRP78 in these cells (Supplementary Fig. S3B). ATF4-depleted macrophages were resistant to ATO-induced impairment of the pathogen engulfment activity (Fig. 1C). Knockdown of ATF4 also led to improved pathogen clearance (Fig. 1D & Supplementary Fig. S2C) and recovery in cytokine production (Fig. 1B).

3.2. ATO-mediated inhibition of CD11b expression is ATF4-dependent

We next asked whether ATO-mediated dysfunction of innate immune response involves ATF4-dependent alterations in macrophage functions. CD11b is an integrin molecule that has been implicated in macrophage functions including phagocytosis and clearance of bacteria and macrophage activation (Pilione et al., 2006). CD11b expression measured as mean fluorescent intensity was significantly reduced in ATO-treated peritoneal macrophages isolated from WT mice but not from $ATF4^{+/-}$ heterozygous mice (Fig. 2A–I). Similar results were also observed in ATO-treated peritoneal macrophages infected with *E. coli* bioparticles

(Fig. 2A–II). Data presented in the line graph (Supplementary Fig. S4) show interaction effects of ATO in *E. coli* infected and non-infected controls in both WT and $ATF4^{+/-}$ heterozygous mice.

ATO-mediated inhibition of $CD11b^+$ expression and ATF4-dependent rescue were also observed following infection with *E. coli* bioparticles in the lung (Fig. 2B). Notably, ATO exposure followed by infection significantly reduced the percentage of infiltrating phagocytic $CD11b^+$ *E. coli*–$FITC^+$ macrophages in the lung tissue as compared to infected but unexposed WT controls (Fig. 2B & 2C). Both percentages and absolute numbers of *E. coli*$^+$$CD11b^+$ cells were significantly reduced in WT mice in response to ATO. Importantly, the observed dysfunction of phagocytic ability of macrophages was rescued in $ATF4^{+/-}$ heterozygous animals. Taken together, ATO has a direct impact on *in vivo* macrophage infiltration and functions that are regulated by ATF4.

3.3. ATO-mediated sustained activation of ATF4 induces apoptosis in murine macrophages

In addition to the demonstration here that impairment of macrophage functions by ATO is dependent on ATF4, we also observed that ATO-induced apoptosis in these target cells contributes to the impaired innate immune responses by eliminating these cells. As shown in Fig. 3A, ATO-treatment in WT mice induced significant induction of apoptosis *in vivo* in $CD11b^+$ cells in the lung tissue as assessed using Annexin-V flow cytometry analysis. The percentage of $CD11b^+$ dead cells was significantly higher in ATO-treated WT mice. These dead $CD11b^+$ cells mainly included macrophages and phagocytic neutrophils (data not shown) suggesting that apoptosis induction of $CD11b^+$ cells by ATO beside their functional impairment in $ATF4^{+/+}$ mice accounts for the reduced efficiency of *E. coli* FITC phagocytosis as observed in the lung tissues of these mice during infection (Fig. 2B & 2C). However, $CD11b^+$ cells were relatively resistant to apoptosis with no significant changes in $CD11b^+$ dead cells in ATO-treated $ATF4^{+/-}$ animals (Fig. 3A). These findings were confirmed in *in vitro* setting using Raw 264.7 cells. There was sustained expression of ATF4 in ATO-treated Raw 264.7 cells, which correlated with increased expression of ATF4-target genes CHOP and GRP78. Increased expression of ATF4 and these UPR-target genes were followed by enhanced cleaved caspase-3 (Fig. 3B). Knocking down of ATF4 by ATF4 siRNA diminishes expression of ATO-induced cleaved caspase-3 (Fig. 3C), suggesting that the cell death was a consequence of ATF4-mediated apoptosis.

3.4. Ca^{++} homeostasis dysregulation underlying ATO-induced apoptosis

We next addressed the molecular mechanisms by which ATO induces apoptosis. Since ER stress is known to release Ca^{++} from ER lumen to the cytoplasm, we tested whether Ca^{++} release persists at later time-points up to 14 h following ATO treatment. A significant increase in the sustained Ca^{++} release was noted (Fig. 4A). Additionally, we observed that this enhanced cytosolic Ca^{++} induced calpain-1/cas-pase-12/caspase-3 signaling pathway and regulated apoptotic macrophage death (Fig. 4B) via IP3R phosphorylation. These ATO-mediated Ca^{++}-dependent responses were similar to those induced by ionophore, an established calcium inducer (Fig. 4C). Furthermore, pretreatment of macrophages with the Ca^{++} chelator, Quin-2; calpain inhibitor, PD-150,607; or Ca^{++} channel, IP3R inhibitor, 2APB; significantly reduced ATO-mediated activation of the calpain pathway and

consequent apoptotic death of the macrophages as viewed by the lowered cleaved caspase-3 (Fig. 4C). These data highlight the importance of ER Ca^{++} release in regulating macrophage survival and viability. It is important to mention here that capase-12 is more relevant to murine models as in humans stress functions are known to be regulated by caspase-4 (Roy et al., 1990; McIlwain et al., 2013).

To address whether Ca^{++}/calpain-1/caspase-12-caspase-3 is uniquely augmented by ATO treatment or other apoptotic death inducing pathways that are also activated in parallel, we investigated the signaling pathways in the mitochondria-regulated death. ATO treatment of Raw 264.7 cells led to increased mROS production (Fig. 5A), coincident with significant decreases in cellular ATP levels (Fig. 5B) that are associated with the loss of MMP (Fig. 5C). ATO-treated cells manifested monomer form which was detected as green fluorescence (Fig. 5C and Supplementary Fig. S5A). The disruption of MMP led to the release of cytochrome *c* from mitochondria to the cytoplasm due to increased permeabilization of the outer mitochondrial membrane (Fig. 5D and Supplementary Fig. S5B). BAX is also known to induce mitochondrial permeability pore and MMP loss (Narita et al., 1998). In this regard, western blot analysis confirmed the localization of BAX from cytoplasm to mitochondria and subsequent release of cytochrome *c* from mitochondria to cytoplasm (Fig. 5E). Here, the fractional purity was confirmed by α/β-tubulin and VDAC proteins for cytoplasmic and mitochondrial fractions respectively. The released cytochrome *c* would then trigger caspase-3-regulated apoptosis. Increased dead cells were validated by the presence of TUNEL positive green cells (Fig. 5F) and induction of Sub-G0 cell populations of cell cycle (Fig. 5G). The cell death may be the result of cumulative contributions from both ER and mitochondrial-mediated death inducing pathways as Ca^{++}/calpain and mitochondrial pathways were simultaneously induced. Since the antioxidant NAC substantially blocked macrophage death (data not shown), ROS are likely important effectors for both of these pathways.

3.5. Small molecule inhibitors of IP3R and VDAC protect against ATO-mediated impairments in macrophage functions by attenuating Ca^{++} homeostasis

Our *in vitro* data highlighted the involvement of ER-Ca^{++} release in ATO-induced macrophage death. Thus, we further investigated the role of Ca^{++} in ATO-impaired macrophage functions. It is known that Ca^{++} channels, IP3R at ER and VDAC at mitochondria are physically linked through the molecular chaperone glucose-regulated protein 75 (GRP75) which facilitate mitochondrial Ca^{++} uptake (Szabadkai et al., 2006). To show the involvement of Ca^{++}, we blocked both IP3R and VDAC channels by using their known inhibitors 2-APB and DIDS respectively. Our data demonstrate that ATO-mediated impairment in fluorescence tagged *E. coli* bioparticles uptake and cytokine release were significantly rescued by the pretreatment of Raw 264.7 cells with 2-APB or Quin 2 (Fig. 6A & B), indicating that Ca^{++} homeostasis is important in the regulation of innate immune functions of the macrophages. Similar protection was also afforded by the pretreatment of these cells with DIDS (Fig. 6A & B). Our data thus demonstrate the importance of ER-mitochondria regulated Ca^{++} homeostasis in ATO-mediated impairment of macrophage functions and subsequent death.

4. Discussion

Arsenic is increasingly being recognized as a suppressor of innate immunity (Kozul et al., 2009a). Environmental exposure to arsenic in adults as well as early life exposures in children contribute to the dys-regulated innate immune functions that have been implicated in persistent opportunistic bacterial and viral infections in exposed individuals (Mazumder et al., 2000; Smith et al., 2006; Raqib et al., 2009; Rahman et al., 2010). However, the mechanisms by which arsenic impairs the immune responses remain undefined.

Earlier, we reported involvement of UPR signaling in arsenic-mediated immune dysregulation with impaired phagocytic functions (Srivastava et al., 2013). ER stress in host cells is known to be associated with bacterial and viral infections (Isler et al., 2005; Tsalikis et al., 2015). ER stress is exploited by infectious organisms to enhance the survival of host cells to favor the proliferation of infectious organism (Lim et al., 2011; Inacio et al., 2015). In this study we identified ATF4, a CREB family transcription factor that facilitates UPR signaling, as a central regulator of host innate immune responses to arsenic. Induced expression of ATF4 and its sustained activation by arsenic triggers calcium-dependent dysregulation of the ER and mitochondria, which is important for the impairment in macrophage functions and apoptotic death of these innate immune cells.

Phagocytes are essential components of the innate immune system. Pattern recognition receptor-mediated signaling and induction of pro-inflammatory cytokines are pre-requisites for efficient phagocytic functions of the macrophages. Our studies show that ATO inhibits the production of IL-1β, IL-10, TGF-β and TNF-α by macrophages and the pro-inflammatory cytokine signaling is rescued in the absence of ATF4 or by interference RNA-mediated knock down of ATF4 in these cells. ATO-mediated inhibition of IL-1β signaling is consistent with the recent observations that inflammasome activation regulated by IL-1β is inhibited by ATO (Maier et al., 2014). The impaired innate immune responses resulting from inefficient inflammasome activation may account for the significant loss of phagocytic activity and pathogen clearance mechanisms of macrophages resulting from ATO exposure.

Importantly, we present a novel role for ATF4 in innate immune regulation following arsenic exposure. In our earlier published study, we demonstrated *in vitro* that arsenic-induced ER stress is associated with dysregulation of innate immune functions of macrophage as prior treatment of macrophage with a chemical chaperone, 4-PBA afforded protection against arsenic-induced impairment in macrophage functions with concomitant diminution of UPR signaling pathway (Srivastava et al., 2013). In this regard, it has been reported that viral infection often induces ER stress (Isler et al., 2005; Zhang et al., 2010; Finnen et al., 2014; Fros et al., 2015). Autophagic responses are also induced by both viral and bacterial infections by a process involving activation of ATF4, which helps host cells to survive during prolonged infection (Wang et al., 2014). For example, during human cytomegalovirus (HCMV) infections, viral protein PUL38 activates the UPR, leading to phosphorylation of PERK and eIF2α and robust accumulation of ATF4, which is important in abrogating cell death by inhibiting JNK phosphorylation (Xuan et al., 2009). Furthermore, ATF4 depletion attenuated virus growth by inhibiting viral gene transcription and DNA synthesis (Qian et al., 2012). Infectious bronchitis virus (IBV) also modulates apoptosis of host cells by

restricting the activation of PERK pathway in UPR signaling (Liao et al., 2013). Thus, while activation of ER stress and ATF4 in host cell following infection enhances survival, our data demonstrate that the same UPR pathway in macrophages reduces innate immune functions and eliminate host defense cells by inducing apoptotic cell death. By depleting ATF4 level in vitro, we demonstrate that arsenic-mediated disruptions of innate functions of macrophage are ATF4-dependent.

Promotion of apoptosis in macrophages in response to arsenic exposure occurs by the sustained activation ATF4. Since we observed that arsenic induces CHOP expression through the PERK/ATF4-dependent pathways, we suggest that the observed apoptotic cell death may be related to CHOP induction. Sustained activation of CHOP is known to induce apoptosis in various biological systems (Nishitoh, 2012; Quick and Faison, 2012). This study points to the involvement of calpain-1, a protease, in the induction of apoptosis. Calpain-1 is known to orchestrate apoptosis in various cell types (Nakagawa and Yuan, 2000). In this regard, we confirmed the involvement of Ca^{++}/calpain-1/caspase-12 pathways in triggering arsenic-induced apoptotic murine macrophage death. We and others previously reported that arsenic toxicity is regulated by ROS generation and mitochondrial signaling (Liu et al., 2001; Le Bras et al., 2005; Liu et al., 2005; Yen et al., 2012). In this manuscript, we confirmed that arsenic also induced mROS in macrophages leading to mitochondrial apoptosis by release of cytochrome *c* from mitochondria to cytoplasm. Taken together, arsenic induces apoptosis in macrophages by multiple death-inducing signaling pathways.

Thus, ATF4 is an important negative regulator of macrophage innate immune functions as depicted in the flow diagram (Fig. 7). Our studies as presented here address a possible mechanism for impairment of innate immune responses resulting from early exposure to ATO. These studies provide mechanistic models for investigating impaired immune regulation during chronic arsenic exposure.

Supplementary Material

Refer to Web version on PubMed Central for supplementary material.

Acknowledgments

This work was partially supported by the Countermeasures Against Chemical Threats (Counteract) program under grant number UO1NS095678 to M.A. The study sponsors had no involvement in the study design, collection, analysis and interpretation of data, the writing of the manuscript and the decision to publish the manuscript. J.S.D. is supported by YCSA 2010 grant from Flight Attendants Medical Research Institute. The authors would like to thank Kenneth P. Hough, Department of Medicine, University of Alabama at Birmingham, for providing assistance in statistical analysis.

References

Abhyankar LN, Jones MR, Guallar E, Navas-Acien A. Arsenic exposure and hypertension: a systematic review. Environ Health Perspect. 2012; 120:494–500. [PubMed: 22138666]

Ahmed S, Ahsan KB, Kippler M, Mily A, Wagatsuma Y, Hoque AM, Ngom PT, El Arifeen S, Raqib R, Vahter M. In utero arsenic exposure is associated with impaired thymic function in newborns possibly via oxidative stress and apoptosis. Toxicol Sci. 2012; 129:305–314. [PubMed: 22713597]

Aranyi C, Bradof JN, O'Shea WJ, Graham JA, Miller FJ. Effects of arsenic trioxide inhalation exposure on pulmonary antibacterial defenses in mice. J Toxicol Environ Health. 1985; 15:163–172. [PubMed: 3884825]

Attardi G, Ching E. Biogenesis of mitochondrial proteins in HeLa cells. Methods Enzymol. 1979; 56:66–79. [PubMed: 459888]

Austyn JM, Gordon S. F4/80, a monoclonal antibody directed specifically against the mouse macrophage. Eur J Immunol. 1981; 11:805–815. [PubMed: 7308288]

Bae HB, Zmijewski JW, Deshane JS, Tadie JM, Chaplin DD, Takashima S, Abraham E. AMP-activated protein kinase enhances the phagocytic ability of macrophages and neutrophils. FASEB J. 2011; 25:4358–4368. [PubMed: 21885655]

Bishayi B, Sengupta M. Intracellular survival of *Staphylococcus aureus* due to alteration of cellular activity in arsenic and lead intoxicated mature Swiss albino mice. Toxicology. 2003; 184:31–39. [PubMed: 12505374]

Biswas R, Ghosh P, Banerjee N, Das JK, Sau T, Banerjee A, Roy S, Ganguly S, Chatterjee M, Mukherjee A, Giri AK. Analysis of T-cell proliferation and cytokine secretion in the individuals exposed to arsenic. Hum Exp Toxicol. 2008; 27:381–386. [PubMed: 18715884]

Brown KG, Ross GL. American Council on, S., Health. Arsenic, drinking water, and health: a position paper of the American Council on Science and Health. Regul Toxicol Pharmacol. 2002; 36:162–174. [PubMed: 12460751]

Burchiel SW, Mitchell LA, Lauer FT, Sun X, McDonald JD, Hudson LG, Liu KJ. Immunotoxicity and biodistribution analysis of arsenic trioxide in C57Bl/6 mice following a 2-week inhalation exposure. Toxicol Appl Pharmacol. 2009; 241:253–259. [PubMed: 19800901]

Cao SS, Kaufman RJ. Unfolded protein response. Curr Biol. 2012; 22:R622–R626. [PubMed: 22917505]

Cardenas A, Smit E, Houseman EA, Kerkvliet NI, Bethel JW, Kile ML. Arsenic exposure and prevalence of the varicella zoster virus in the United States: NHANES (2003–2004 and 2009–2010). Environ Health Perspect. 2015

Cornejo VH, Pihan P, Vidal RL, Hetz C. Role of the unfolded protein response in organ physiology: lessons from mouse models. IUBMB Life. 2013; 65:962–975. [PubMed: 24227223]

Deshane J, Zmijewski JW, Luther R, Gaggar A, Deshane R, Lai JF, Xu X, Spell M, Estell K, Weaver CT, Abraham E, Schwiebert LM, Chaplin DD. Free radical-producing myeloid-derived regulatory cells: potent activators and suppressors of lung inflammation and airway hyperresponsiveness. Mucosal Immunol. 2011; 4:503–518. [PubMed: 21471960]

Finnen RL, Hay TJ, Dauber B, Smiley JR, Banfield BW. The herpes simplex virus 2 virion-associated ribonuclease vhs interferes with stress granule formation. J Virol. 2014; 88:12727–12739. [PubMed: 25142597]

Fros JJ, Major LD, Scholte FE, Gardner J, van Hemert MJ, Suhrbier A, Pijlman GP. Chikungunya virus non-structural protein 2-mediated host shut-off disables the unfolded protein response. J Gen Virol. 2015; 96:580–589. [PubMed: 25395592]

Gibb H, Haver C, Gaylor D, Ramasamy S, Lee JS, Lobdell D, Wade T, Chen C, White P, Sams R. Utility of recent studies to assess the National Research Council 2001 estimates of cancer risk from ingested arsenic. Environ Health Perspect. 2011; 119:284–290. [PubMed: 21030336]

Inacio P, Zuzarte-Luis V, Ruivo MT, Falkard B, Nagaraj N, Rooijers K, Mann M, Mair G, Fidock DA, Mota MM. Parasite-induced ER stress response in hepatocytes facilitates Plasmodium liver stage infection. EMBO Rep. 2015

Isler JA, Skalet AH, Alwine JC. Human cytomegalovirus infection activates and regulates the unfolded protein response. J Virol. 2005; 79:6890–6899. [PubMed: 15890928]

Jo H, Choe SS, Shin KC, Jang H, Lee JH, Seong JK, Back SH, Kim JB. ER stress induces hepatic steatosis via increased expression of the hepatic VLDL receptor. Hepatology. 2012

Kile ML, Houseman EA, Baccarelli AA, Quamruzzaman Q, Rahman M, Mostofa G, Cardenas A, Wright RO, Christiani DC. Effect of prenatal arsenic exposure on DNA methylation and leukocyte subpopulations in cord blood. Epigenetics. 2014; 9:774–782. [PubMed: 24525453]

Kozul CD, Ely KH, Enelow RI, Hamilton JW. Low-dose arsenic compromises the immune response to influenza A infection in vivo. Environ Health Perspect. 2009a; 117:1441–1447. [PubMed: 19750111]

Kozul CD, Hampton TH, Davey JC, Gosse JA, Nomikos AP, Eisenhauer PL, Weiss DJ, Thorpe JE, Ihnat MA, Hamilton JW. Chronic exposure to arsenic in the drinking water alters the expression of immune response genes in mouse lung. Environ Health Perspect. 2009b; 117:1108–1115. [PubMed: 19654921]

Le Bras M, Clement MV, Pervaiz S, Brenner C. Reactive oxygen species and the mitochondrial signaling pathway of cell death. Histol Histopathol. 2005; 20:205–219. [PubMed: 15578439]

Lengfelder E, Hofmann WK, Nowak D. Impact of arsenic trioxide in the treatment of acute promyelocytic leukemia. Leukemia. 2012; 26:433–442. [PubMed: 21904379]

Liao Y, Fung TS, Huang M, Fang SG, Zhong Y, Liu DX. Upregulation of CHOP/GADD153 during coronavirus infectious bronchitis virus infection modulates apoptosis by restricting activation of the extracellular signal-regulated kinase pathway. J Virol. 2013; 87:8124–8134. [PubMed: 23678184]

Lim YJ, Choi JA, Choi HH, Cho SN, Kim HJ, Jo EK, Park JK, Song CH. Endoplasmic reticulum stress pathway-mediated apoptosis in macrophages contributes to the survival of *Mycobacterium tuberculosis*. PLoS One. 2011; 6:e28531. [PubMed: 22194844]

Liu SX, Athar M, Lippai I, Waldren C, Hei TK. Induction of oxyradicals by arsenic: implication for mechanism of genotoxicity. Proc Natl Acad Sci U S A. 2001; 98:1643–1648. [PubMed: 11172004]

Liu SX, Davidson MM, Tang X, Walker WF, Athar M, Ivanov V, Hei TK. Mitochondrial damage mediates genotoxicity of arsenic in mammalian cells. Cancer Res. 2005; 65:3236–3242. [PubMed: 15833855]

Maier NK, Crown D, Liu J, Leppla SH, Moayeri M. Arsenic trioxide and other arsenical compounds inhibit the NLRP1, NLRP3, and NAIP5/NLRC4 inflammasomes. J Immunol. 2014; 192:763–770. [PubMed: 24337744]

Martin-Chouly C, Morzadec C, Bonvalet M, Galibert MD, Fardel O, Vernhet L. Inorganic arsenic alters expression of immune and stress response genes in activated primary human T lymphocytes. Mol Immunol. 2011; 48:956–965. [PubMed: 21281968]

Masuoka HC, Townes TM. Targeted disruption of the activating transcription factor 4 gene results in severe fetal anemia in mice. Blood. 2002; 99:736–745. [PubMed: 11806972]

Mazumder DN, Haque R, Ghosh N, De BK, Santra A, Chakraborti D, Smith AH. Arsenic in drinking water and the prevalence of respiratory effects in West Bengal, India. Int J Epidemiol. 2000; 29:1047–1052. [PubMed: 11101546]

McClintock TR, Chen Y, Bundschuh J, Oliver JT, Navoni J, Olmos V, Lepori EV, Ahsan H, Parvez F. Arsenic exposure in Latin America: biomarkers, risk assessments and related health effects. Sci Total Environ. 2012; 429:76–91. [PubMed: 22119448]

McIlwain DR, Berger T, Mak TW. Caspase functions in cell death and disease. Cold Spring Harb Perspect Biol. 2013; 5:a008656. [PubMed: 23545416]

Mink PJ, Alexander DD, Barraj LM, Kelsh MA, Tsuji JS. Low-level arsenic exposure in drinking water and bladder cancer: a review and meta-analysis. Regul Toxicol Pharmacol. 2008; 52:299–310. [PubMed: 18783726]

Nakagawa T, Yuan J. Cross-talk between two cysteine protease families. Activation of caspase-12 by calpain in apoptosis. J Cell Biol. 2000; 150:887–894. [PubMed: 10953012]

Narita M, Shimizu S, Ito T, Chittenden T, Lutz RJ, Matsuda H, Tsujimoto Y. Bax interacts with the permeability transition pore to induce permeability transition and cytochrome c release in isolated mitochondria. Proc Natl Acad Sci U S A. 1998; 95:14681–14686. [PubMed: 9843949]

Nayak AS, Lage CR, Kim CH. Effects of low concentrations of arsenic on the innate immune system of the zebrafish (*Danio rerio*). Toxicol Sci. 2007; 98:118–124. [PubMed: 17400579]

Nishitoh H. CHOP is a multifunctional transcription factor in the ER stress response. J Biochem. 2012; 151:217–219. [PubMed: 22210905]

Nouri K, Ricotti CA Jr, Bouzari N, Chen H, Ahn E, Bach A. The incidence of recurrent herpes simplex and herpes zoster infection during treatment with arsenic trioxide. J Drugs Dermatol. 2006; 5:182–185. [PubMed: 16485889]

Patterson R, Vega L, Trouba K, Bortner C, Germolec D. Arsenic-induced alterations in the contact hypersensitivity response in Balb/c mice. Toxicol Appl Pharmacol. 2004; 198:434–443. [PubMed: 15276424]

Pilione MR, Agosto LM, Kennett MJ, Harvill ET. CD11b is required for the resolution of inflammation induced by *Bordetella bronchiseptica* respiratory infection. Cell Microbiol. 2006; 8:758–768. [PubMed: 16611225]

Pion M, Stalder R, Correa R, Mangeat B, Towers GJ, Piguet V. Identification of an arsenic-sensitive block to primate lentiviral infection of human dendritic cells. J Virol. 2007; 81:12086–12090. [PubMed: 17728230]

Qian Z, Xuan B, Chapa TJ, Gualberto N, Yu D. Murine cytomegalovirus targets transcription factor ATF4 to exploit the unfolded-protein response. J Virol. 2012; 86:6712–6723. [PubMed: 22496230]

Qing G, Li B, Vu A, Skuli N, Walton ZE, Liu X, Mayes PA, Wise DR, Thompson CB, Maris JM, Hogarty MD, Simon MC. ATF4 regulates MYC-mediated neuroblastoma cell death upon glutamine deprivation. Cancer Cell. 2012; 22:631–644. [PubMed: 23153536]

Quick QA, Faison MO. CHOP and caspase 3 induction underlie glioblastoma cell death in response to endoplasmic reticulum stress. Exp Ther Med. 2012; 3:487–492. [PubMed: 22969916]

Rahman A, Persson LA, Nermell B, El Arifeen S, Ekstrom EC, Smith AH, Vahter M. Arsenic exposure and risk of spontaneous abortion, stillbirth, and infant mortality. Epidemiology. 2010; 21:797–804. [PubMed: 20864889]

Rahman A, Vahter M, Ekstrom EC, Persson LA. Arsenic exposure in pregnancy increases the risk of lower respiratory tract infection and diarrhea during infancy in Bangladesh. Environ Health Perspect. 2011; 119:719–724. [PubMed: 21147604]

Raqib R, Ahmed S, Sultana R, Wagatsuma Y, Mondal D, Hoque AM, Nermell B, Yunus M, Roy S, Persson LA, Arifeen SE, Moore S, Vahter M. Effects of in utero arsenic exposure on child immunity and morbidity in rural Bangladesh. Toxicol Lett. 2009; 185:197–202. [PubMed: 19167470]

Roy B, Fujimoto N, Ito A. Growth-promoting effect of retinoic acid in transplantable pituitary tumor of rat. Jpn J Cancer Res. 1990; 81:878–883. [PubMed: 2172196]

Smith AH, Marshall G, Yuan Y, Ferreccio C, Liaw J, von Ehrenstein O, Steinmaus C, Bates MN, Selvin S. Increased mortality from lung cancer and bronchiectasis in young adults after exposure to arsenic in utero and in early childhood. Environ Health Perspect. 2006; 114:1293–1296. [PubMed: 16882542]

Smith AH, Marshall G, Yuan Y, Liaw J, Ferreccio C, Steinmaus C. Evidence from Chile that arsenic in drinking water may increase mortality from pulmonary tuberculosis. Am J Epidemiol. 2011; 173:414–420. [PubMed: 21190988]

Soto-Pena GA, Luna AL, Acosta-Saavedra L, Conde P, Lopez-Carrillo L, Cebrian ME, Bastida M, Calderon-Aranda ES, Vega L. Assessment of lymphocyte subpopulations and cytokine secretion in children exposed to arsenic. FASEB J. 2006; 20:779–781. [PubMed: 16461332]

Srivastava RK, Kaylani SZ, Edrees N, Li C, Talwelkar SS, Xu J, Palle K, Pressey JG, Athar M. GLI inhibitor GANT-61 diminishes embryonal and alveolar rhabdo-myosarcoma growth by inhibiting Shh/AKT-mTOR axis. Oncotarget. 2014; 5:12151–12165. [PubMed: 25432075]

Srivastava RK, Li C, Chaudhary SC, Ballestas ME, Elmets CA, Robbins DJ, Matalon S, Deshane JS, Afaq F, Bickers DR, Athar M. Unfolded protein response (UPR) signaling regulates arsenic trioxide-mediated macrophage innate immune function disruption. Toxicol Appl Pharmacol. 2013; 272:879–887. [PubMed: 23954561]

Szabadkai G, Bianchi K, Varnai P, De Stefani D, Wieckowski MR, Cavagna D, Nagy AI, Balla T, Rizzuto R. Chaperone-mediated coupling of endoplasmic reticulum and mitochondrial Ca2+ channels. J Cell Biol. 2006; 175:901–911. [PubMed: 17178908]

Tanvetyanon T, Nand S. Herpes zoster during treatment with arsenic trioxide. Ann Hematol. 2004; 83:198–200. [PubMed: 15064871]

Tohyama N, Tanaka S, Onda K, Sugiyama K, Hirano T. Influence of anticancer agents on cell survival, proliferation, and CD4 + CD25 + Foxp3+ regulatory T cell-frequency in human peripheral-blood mononuclear cells activated by T cell-mitogen. Int Immunopharmacol. 2013; 15:160–166. [PubMed: 23178575]

Tsalikis J, Tattoli I, Ling A, Sorbara MT, Croitoru DO, Philpott DJ, Girardin SE. Intracellular bacterial pathogens trigger the formation of U bodies through metabolic stress induction. J Biol Chem. 2015

Walter P, Ron D. The unfolded protein response: from stress pathway to homeo-static regulation. Science. 2011; 334:1081–1086. [PubMed: 22116877]

Wang J, Kang R, Huang H, Xi X, Wang B, Wang J, Zhao Z. Hepatitis C virus core protein activates autophagy through EIF2AK3 and ATF6 UPR pathway-mediated MAP1LC3B and ATG12 expression. Autophagy. 2014; 10:766–784. [PubMed: 24589849]

Wang W, Lian N, Li L, Moss HE, Wang W, Perrien DS, Elefteriou F, Yang X. Atf4 regulates chondrocyte proliferation and differentiation during endochondral ossification by activating Ihh transcription. Development. 2009; 136:4143–4153. [PubMed: 19906842]

Wang W, Lian N, Ma Y, Li L, Gallant RC, Elefteriou F, Yang X. Chondrocytic Atf4 regulates osteoblast differentiation and function via Ihh. Development. 2012; 139:601–611. [PubMed: 22190639]

Woo CW, Cui D, Arellano J, Dorweiler B, Harding H, Fitzgerald KA, Ron D, Tabas I. Adaptive suppression of the ATF4-CHOP branch of the unfolded protein response by toll-like receptor signalling. Nat Cell Biol. 2009; 11:1473–1480. [PubMed: 19855386]

Xuan B, Qian Z, Torigoi E, Yu D. Human cytomegalovirus protein pUL38 induces ATF4 expression, inhibits persistent JNK phosphorylation, and suppresses endoplasmic reticulum stress-induced cell death. J Virol. 2009; 83:3463–3474. [PubMed: 19193809]

Yamakura M, Tsuda K, Ugai T, Sugihara H, Nisihida Y, Takeuchi M, Matsue K. High frequency of varicella zoster virus reactivation associated with the use of arsenic trioxide in patients with acute promyelocytic leukemia. Acta Haematol. 2014; 131:76–77. [PubMed: 24081111]

Yen YP, Tsai KS, Chen YW, Huang CF, Yang RS, Liu SH. Arsenic induces apoptosis in myoblasts through a reactive oxygen species-induced endoplasmic reticulum stress and mitochondrial dysfunction pathway. Arch Toxicol. 2012; 86:923–933. [PubMed: 22622864]

Zhang F, Moon A, Childs K, Goodbourn S, Dixon LK. The African swine fever virus DP71L protein recruits the protein phosphatase 1 catalytic subunit to dephosphorylate eIF2alpha and inhibits CHOP induction but is dispensable for these activities during virus infection. J Virol. 2010; 84:10681–10689. [PubMed: 20702639]

Zhou LF, Zhu Y, Cui XF, Xie WP, Hu AH, Yin KS. Arsenic trioxide, a potent inhibitor of NF-kappaB, abrogates allergen-induced airway hyperresponsiveness and inflammation. Respir Res. 2006; 7:146. [PubMed: 17178007]

Appendix A. Supplementary data

Supplementary data to this article can be found online at http://dx.doi.org/10.1016/j.taap.2016.07.015.

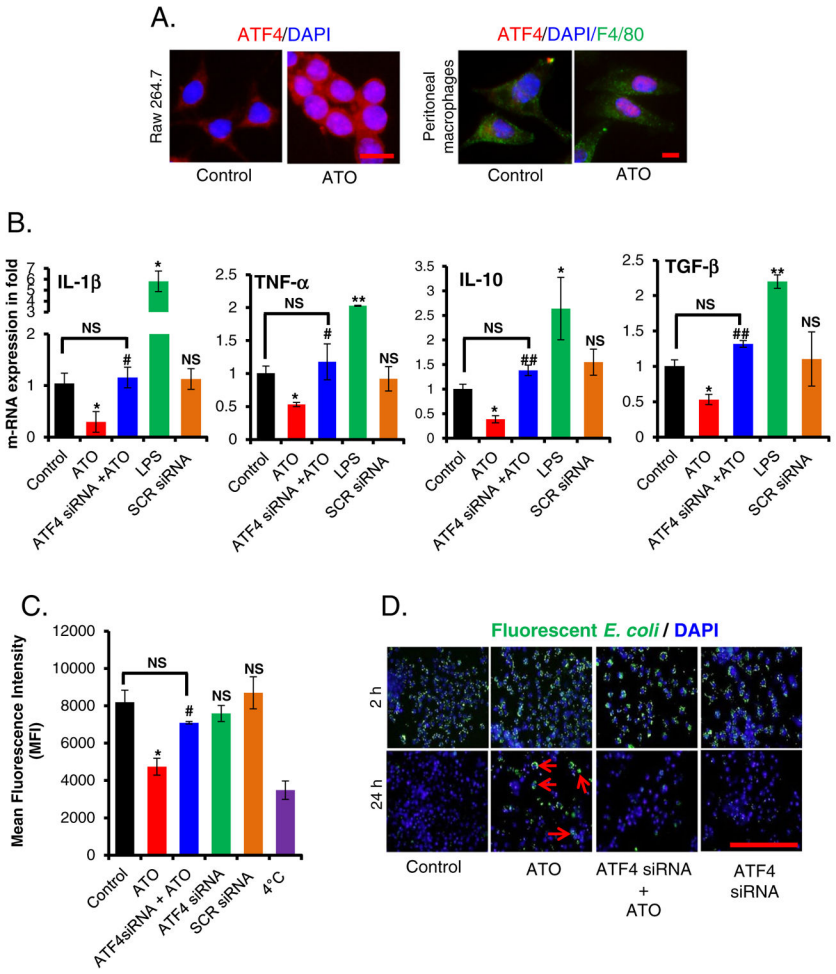

Fig. 1.

ATO-inhibited cytokine production, bacterial engulfment and its clearance of engulfed bacteria in murine macrophage in ATF4-dependent manner. (A) Immunofluorescence staining showing migration and localization of ATF4 (red) from cytosol to nucleus in ATO (2 μM for 14 h)-treated Raw 264.7 cells (bar, 50 μm) and in peritoneal macrophages (F4/80, green) (bar, 25 μm) isolated from WT mice. Nuclei were stained with DAPI. (B) Histograms showing real time PCR analysis of mRNAs expression encoding the indicated cytokines in ATF4 siRNA or scrambled siRNA-transfected Raw 264.7 cells treated either with saline (control) or with ATO (2 μM for 14 h). Treatment of the cells with LPS (100 ng for 3 h) served as a positive control. (C) ATF4 siRNA- or scrambled siRNA-transfected Raw 264.7 cells were treated either with saline or with ATO (2 μM for 14 h), followed by incubation with fluorescently labeled rabbit-IgG coated latex beads with for 45 min at 37 °C. Histogram showing mean fluorescence intensity of engulfed fluorescent beads (recorded at excitation 485 nm and emission at 535 nm by microplate reader). Negative control cells received identical treatments as described above except were incubated at 4 °C instead of 37 °C. (D) Infection load of fluorescently labeled opsonized *E. coli* bioparticles in Raw 264.7 cells was recorded at 2 h and 24 h using fluorescent microscopy (bar, 200 μm). Arrows indicating the presence of *E. coli* bioparticles. Data are expressed as mean ± SEM. **P* < 0.05, compared to

control. $^{\#}P < 0.05$ and $^{\#\#}P < 0.01$, compared to ATO-treated group. NS-nonsignificant compared to control.

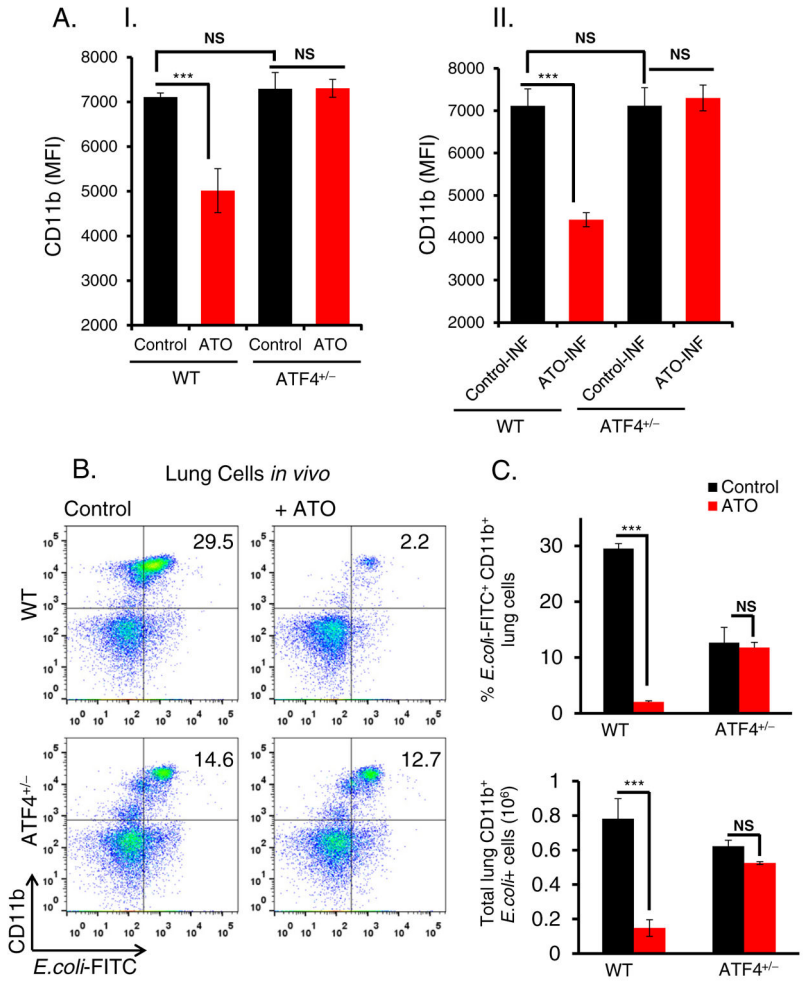

Fig. 2.

ATO down regulates CD11b expression in ATF4-dependent manner. (A); (A–I) Histogram showing mean fluorescent intensity of CD11b expression determined by flow cytometry analysis of peritoneal macrophages, isolated from WT and ATF4$^{+/-}$heterozygous mice. These macrophages were treated with either saline (control) or ATO (2 μM for 14 h). (A–II) Similar experiments were also performed by infecting (INF) macrophages with *E. coli* fluorescents conjugated bioparticles. For this study, following treatment with ATO (2 μM for 14 h), peritoneal macrophages were incubated with *E. coli* (bacterial: cell, 50:1 ratio) at 37 °C for 2 h and then cells were washed twice with PBS followed by flow cytometry analysis. (B) Flow cytometry analysis of lung infiltrates of WT and ATF4$^{+/-}$ heterozygous mice treated intraperitoneally with either saline (control) or ATO (50 μg/mouse in 200 μl PBS; daily for 10 days) and then intratracheally infected with *E. coli*-FITC. Representative dot plots showing percentages of CD11b + *E. coli*-FITC^{+} cells in the lung tissues. (C) Histogram showing percent *E. coli* FITC^{+}CD11b^{+} cells (top panel) and absolute numbers of *E. coli*-FITC^{+} CD11b^{+} cells (lower panel) in lung tissues. Data are expressed as mean ± SEM. ***$P < 0.001$ compared to their respective controls. NS-nonsignificant.

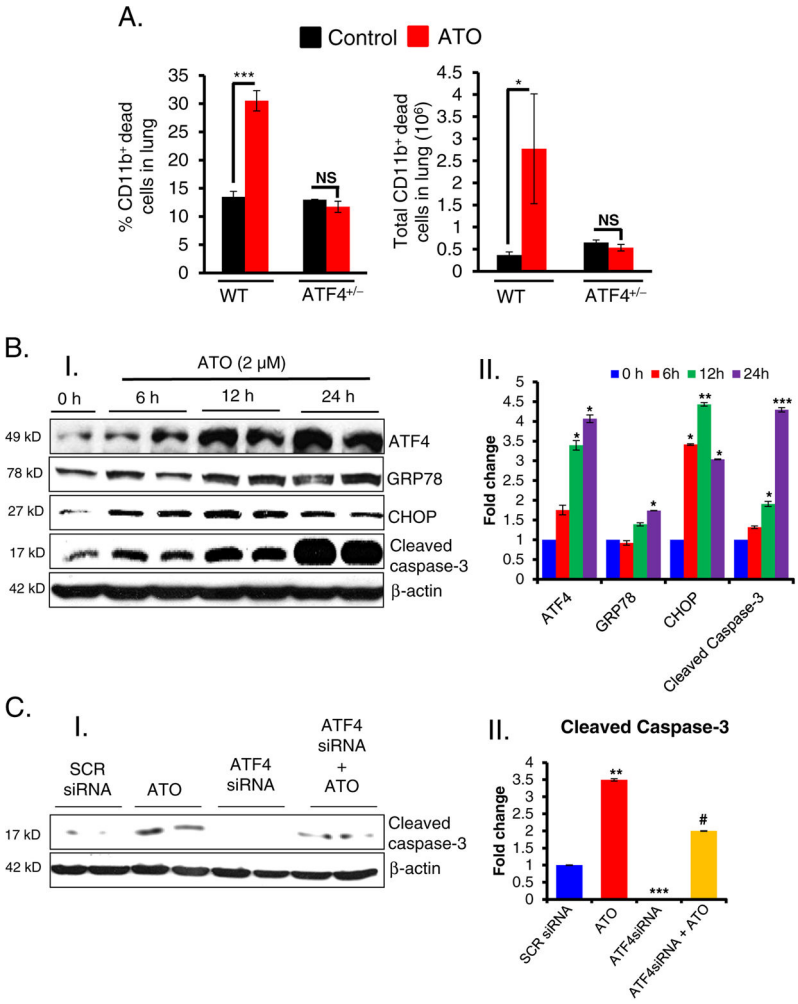

Fig. 3.

ATO-induced apoptosis in murine macrophages. Histogram showing the percentage and total dead $CD11b^+$ cells in the lung tissues of WT and $ATF4^{+/-}$heterozygous mice. These mice were treated with either saline or ATO (50 μg/mouse in 200 μl PBS, intra-peritoneal; daily for 10 days) and then intratracheally infected with *E. coli*-FITC as referred to the Material & methods section. (B); (B–I) Western blot analysis of ATF4, GRP78, CHOP and cleaved caspse-3 in ATO-treated Raw 264.7 cells. (B–II) Histogram representing the densitometry analysis of western blots. (C); (C–I) Western blots analysis of cleaved caspase-3 in ATF4 knockdown cells treated with either saline or ATO (2 μM). Scrambled (SCR) siRNA was used as a negative control. (C–II) Histogram representing the densitometry analysis of western blots. Data are expressed as mean ± SEM. $*P < 0.05$, $**P < 0.01$, $***P < 0.001$ compared to their respective controls. $^{\#}P < 0.05$ compared to ATO-treated group. NS-nonsignificant.

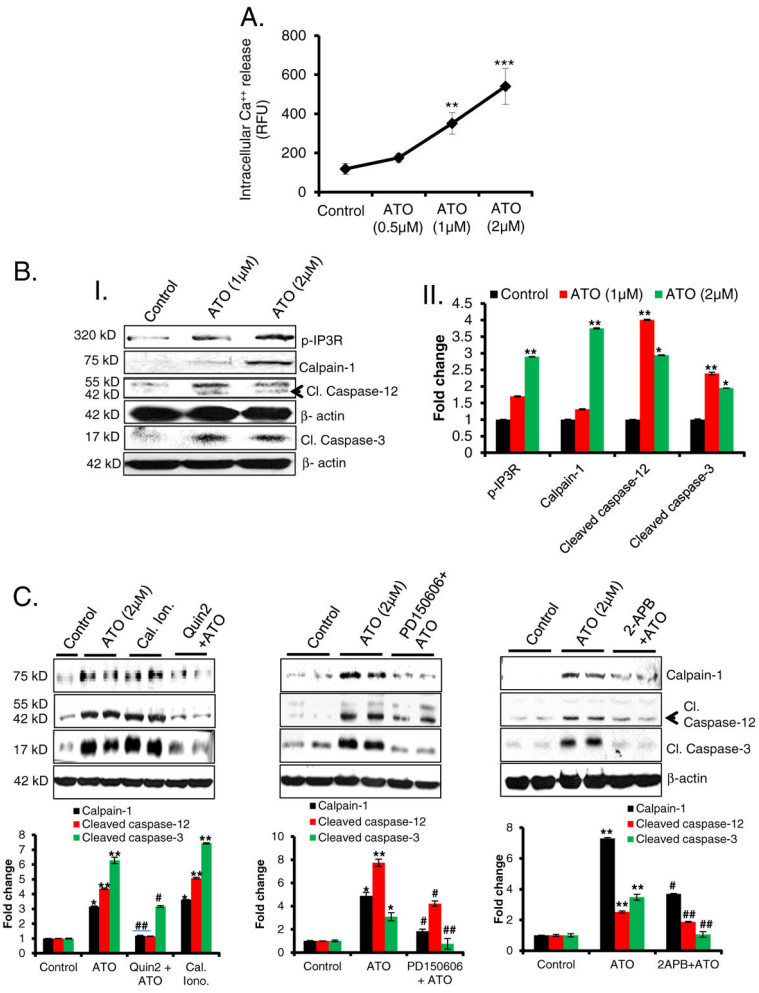

Fig. 4.

ATO-mediated apoptosis is regulated by Ca^{++}/calpain-1/caspase-12-mediated apoptosis. (A) Line graph showing intracellular Ca^{++} release from ATO-treated Raw 264.7 cells at 14 h. Fluorescence intensity was recorded at excitation wavelength 494 nm and emission wavelength 516 nm using a microplate reader and expressed as mean of relative fluorescence unit (RFU). (B); (B–I) Western blot analysis for p-IP3R, calpain-1, cleaved caspase-12, and cleaved caspase-3 proteins in lysates prepared from ATO-treated (1 and 2 μM for 24 h) Raw 264.7 cells. (B–II) Histogram representing the densitometry analysis of western blots. (C) Western blot analysis for calpain-1, cleaved caspase-12 and cleaved caspase-3 proteins in ATO-treated Raw 264.7 cell lysate. These cells were pretreated with calcium chelator, Quin2 (20 μM for 3 h) or calpain inhibitor, PD150606 (10 μM for 3 h) or IP3R inhibitor, 2-APB (20 μM, 6 h). In these experiments calcium ionophore (cal. iono.), (2 μM for 3 h) was used as positive control to address whether the effects are indeed Ca^{++} regulated. Histograms representing the densitometry analysis of western blots. Data are expressed as mean ± SEM. $^{*}P < 0.05$, $^{**}P < 0.01$, $^{***}P < 0.001$ compared to control. $^{\#}P < 0.05$, $^{\#\#}P < 0.01$, compared to ATO-treated group.

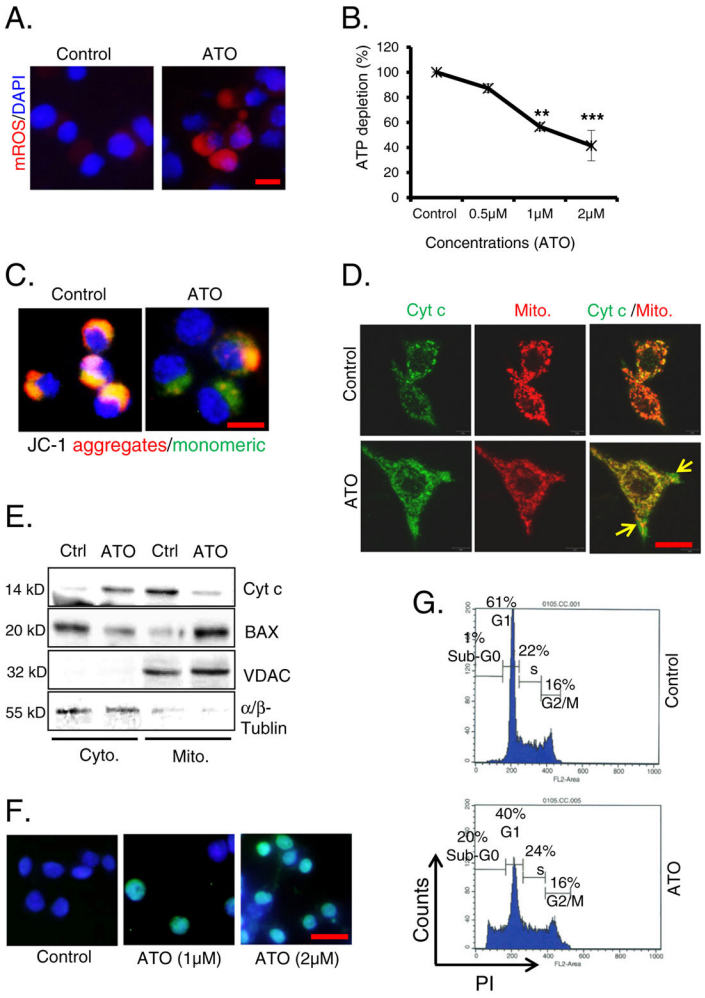

Fig. 5.

ATO-mediated apoptosis is regulated by mitochondrial signaling pathways. (A) Mitochondrial ROS (mROS) production in saline and ATO-treated (2 μM for 24 h) Raw 264.7 (bar, 30 μm). (B) Line graph showing ATP depletion in ATO-treated Raw 264.7 cells in comparison to saline-treated control cells. (C) Loss of MMP was observed using JC-1 dye in ATO-treated (2 μM for 24 h) cells under fluorescence microscope as assessed by the changes in the ratio of red (dye aggregates) to green (monomer) fluorescence (bar, 50 μm). (D) Immunofluorescence staining of ATO-induced release of cytochrome *c* (Cyt c) (green) in cytoplasm from mitochondria (red). Mitochondria were stained with mitotracker, a red dye (250 nM for 20 min) (bar, 50 μm). (E) Western blot analysis of ATO-induced alterations of Cyt c and BAX levels in cytoplasm and mitochondria. Fraction purity was confirmed by α/β-tubulin and VDAC proteins for cytoplasmic (Cyto.) and mitochondrial (Mito.) fractions respectively. (F) TUNEL assay was performed in ATO-treated (1 & 2 μM for 24 h) Raw 264.7 cells. Green fluorescence positive cells represent apoptotic cells (bar, 50 μm). (G) Apoptosis was also recorded by flow cytometry. Sub-G0 population of cells treated with ATO (2 μM for 24 h) represented apoptotic cells. Data are expressed as mean ± SE. $^{**}P < 0.01$ and $^{***}P < 0.001$ show significance levels compared to control.

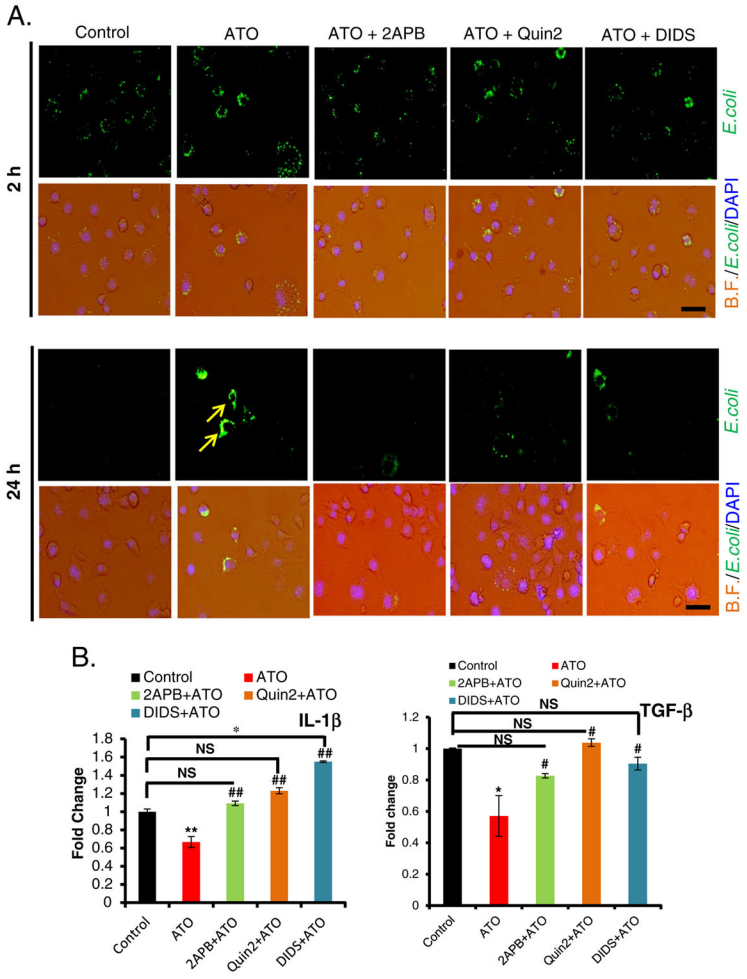

Fig. 6.

Treatment with 2-APB, Quin2 or DIDS attenuated ATO-induced impairment in macrophage functions disruption. (A) Overlay of microphotographs on bright filed (B.F.) and green channel (*E. coli*) with DAPI showing protection afforded by 2-APB (20 μM 6 h), Quin2 (20 μM, 3 h) and DIDS (200 μM, 6 h) against ATO-mediated (2 μM, 14 h) disruption of fluorescent *E. coli* bioparticles clearance (marked by arrows) at 24 h. Infection load of fluorescently labeled *E. coli* bioparticles were observed under the microscope at 2 h and 24 h after various treatments to Raw 264.7 cells (bar, 100 μm). (B) Histograms showing real time PCR analysis of cytokines IL-1β and TGF-β. Blocking IP3R or VDAC channel by 2-APB or DIDS, or chelating Ca^{++} by Quin2, significantly restored the level of diminished mRNA expression of cytokines in ATO-treated Raw 264.7 cells. Data are expressed as mean ± SE. $^{*}P < 0.05$, $^{**}P < 0.01$ compared to their respective controls. $^{\#}P < 0.05$, $^{\#\#}P < 0.01$ compared to ATO-treated group. NS-nonsignificant.

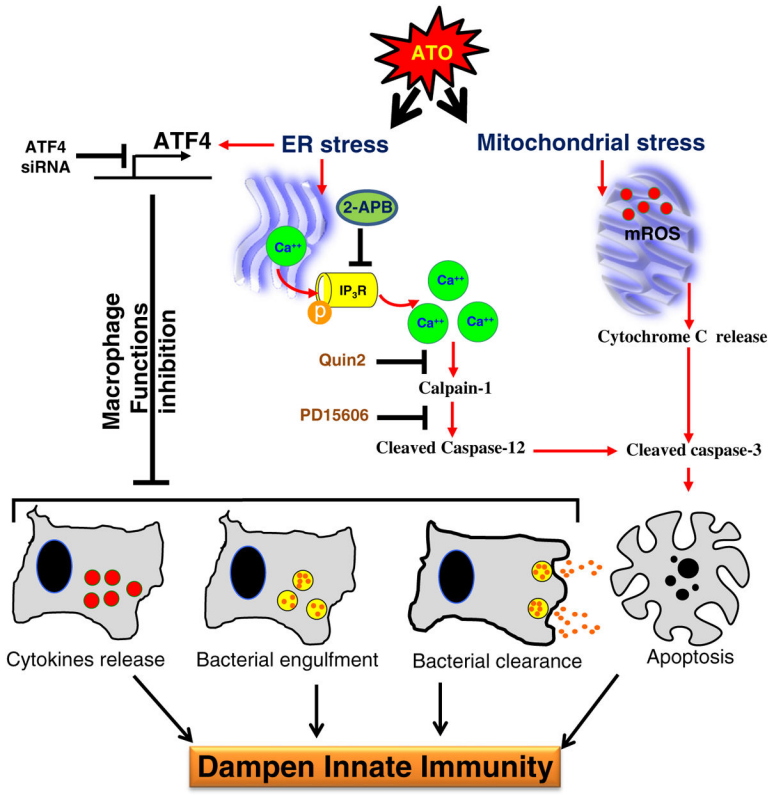

Fig. 7.

Flow diagram depicting the mechanism by which ATO treatment blocks macrophage functions and induces apoptosis in ATF4-dependent manner. ATO activates ATF4, a UPR signaling transcription factor, in murine macrophages, which dysregulates multiple macrophage functions including cytokines release, bacterial engulfment and clearance of engulfed bacteria. In ATO-treated macrophages, sustained activation of ATF4 leads to apoptosis via multiple pathways. Ca^{++}-dependent calpain-1/caspase-12-mediated apoptosis and mitochondrial-dependent apoptosis via release of cytochrome-c from mitochondria to cytoplasm have been recorded. Overall, these effects may lead to dampening of macrophage-dependent innate immune responses. The role of ATF4 in ATO-mediated macrophage dysregulation was ascertained by the genetic approaches where knocking down of ATF4 afforded significantly protection against ATO-mediated impairment of macrophage functions. Role of calcium homeostasis in this toxicity could be confirmed by the treatment of these macrophages with Ca^{++} channel blocker or Ca^{++} chelators which attenuated ATO-induced calpain-1/caspase-12-mediated apoptosis and perhaps other functions related to ATF4 activation.